Journal of Computational and Applied Mechanics, Vol. 5., No. 2., (2004), pp. 323–335

STUDY OF BLADE TO BLADE FLOWS AND CIRCUMFERENTIAL STALL PROPAGATION IN RADIAL DIFFUSERS AND RADIAL FANS BY VORTEX CLOUD ANALYSIS

R. Ivan Lewis
University of Newcastle
Newcastle upon Tyne, NE1 7RU
r.i.lewis@ncl.ac.uk

[Received: October 14, 2004]

Abstract. The objective of this paper is extension of vortex cloud simulation to the study of deep rotating stall cell propagation in radial turbomachines. Previous studies [1][2] provided the basic analysis, summarized in part here, for radial and mixed-flow blade rows but with identical blade-to-blade flow. Lifting of this restriction here permits the natural development of circumferential flow variations, revealing the growth of major upstream rotating stall cells for a radial diffuser with ten log-spiral blades but with high angle of attack (deep stall). For the same blade row run as a radial fan, however, stall cell formation and propagation is found to be inhibited. Additional studies are included for a cambered blade geometry typical of axial compressors. Used as an eight bladed radial diffuser, classical rotating stall is predicted. When operated as a rotor, rotating is again inhibited and modified.

Mathematical Subject Classification: 76B47, 76M23
Keywords: radial turbomachines, rotating stall, vortex dynamics

1. Introduction

A full statement and development of the underlying equations for vortex cloud simulation of mixed-flow and radial turbomachines have been given in previous presentations [1][2] and a brief summary only of these techniques will be given here. A detailed exposition of the underlying methodology of vortex cloud analysis has been given in ref. [3] and a more recent review of numerical developments and applications in ref. [4]. First, the basic equations for surface vorticity flow modelling will be given in Sections 2 & 3 including extension to vortex cloud modelling of turbomachine linear cascades. Second, the transformation techniques for applying these equations to radial cascades will be summarized in Section 4. Investigations of the stalling flow of a ten bladed radial diffuser will also be studied in Section 4, followed by studies of an identical blade row run as a fan rotor, Section 5. A second radial blade row will be considered in Section 6 based on typical axial compressor geometry with a cambered blade profile. A summary of conclusions will follow in Section 7.

2. Vorticity modelling of cascades

The fundamental basis of vortex element representation of the Navier-Stokes equations has been given by the author [3], beginning with the boundary integral equation for potential flow past an arbitrary body, equation (1), with reference

$$\tfrac{1}{2}\gamma(s_m) + \oint k(s_m, s_n)\gamma(s_n)\mathrm{d}s_n + \\ + W_\infty(\cos\alpha_\infty \cos\beta_m + \sin\alpha_\infty \sin\beta_m) = 0 \qquad (1)$$

where, for the boundary condition of zero internal velocity inside the body, the surface velocity v_{sn} is equal to the surface vorticity $\gamma(\mathrm{s}_n)$.

$$v_{sn} = \gamma(s_n) \qquad (2)$$

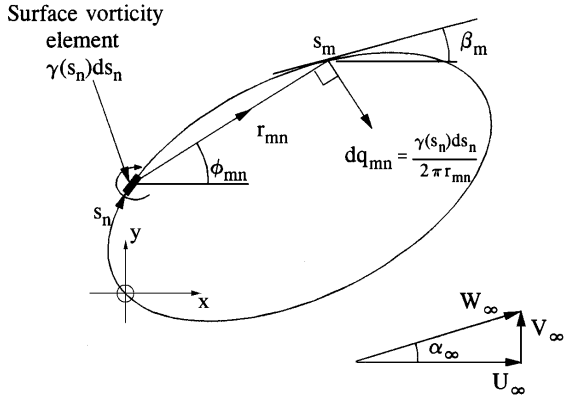

Figure 1. Surface vorticity model for flow past a body in a uniform stream W_∞

The coupling coefficient $k(s_m, s_n)$ linking points m & n on the body surface is given by

$$k(s_m, s_n) = \frac{1}{2\pi}\left\{\frac{(y_m - y_n)\cos\beta_m - (x_m - x_n)\sin\beta_m}{(x_m - x_n)^2 + (y_m - y_n)^2}\right\} . \qquad (3)$$

For a turbomachine cascade blade periodic in the y direction with pitch t, this becomes

$$k(s_m, s_n) = \frac{1}{2t}\left\{\frac{\sin\frac{2\pi}{t}(y_m - y_n)\cos\beta_m - \sinh\frac{2\pi}{t}(x_m - x_n)\sin\beta_m}{\cosh\frac{2\pi}{t}(x_m - x_n) - \cos\frac{2\pi}{t}(y_m - y_n)}\right\} . \qquad (4)$$

The standard numerical strategy is to represent the body surface by M discrete elements as shown in Figure 2, whereupon equation (1) transforms to the set of M linear equations

$$\sum_1^M K(s_m, s_n)\gamma(s_n) = -U_\infty \cos\beta_m - V_\infty \sin\beta_m . \qquad (5)$$

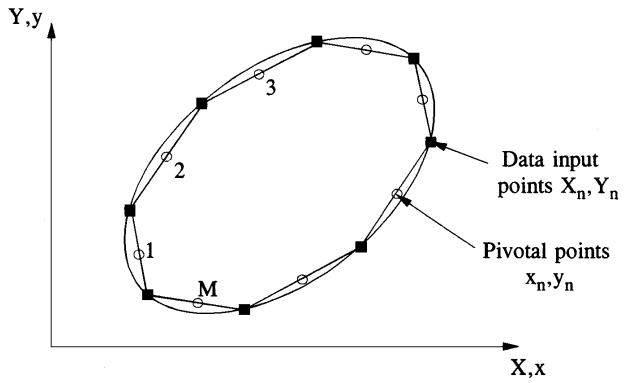

Figure 2. Numerical discretisation of the body surface

The revised coupling coefficients are then given by

$$K(s_m, s_n) = k(s_m, s_n)\Delta s_n \ . \tag{6}$$

These equations are of course only applicable to inviscid/potential flows, but may be extended to handle viscous fluids by vortex dynamics modelling, for which additional terms appear on the right hand side to account for the influence of the distributed vorticity of the external flow field. Thus we have

$$\begin{aligned} \sum_{1}^{M} K(s_m, s_n)\gamma(s_n) = &-U_\infty \cos\beta_m - V_\infty \sin\beta_m \\ &- \sum_{j=1}^{Z} \Delta\Gamma_j (U_{mj}\cos\beta_m + V_{mj}\sin\beta_m) \end{aligned} \ , \tag{7}$$

where the spatially distributed vorticity has been discretised into a large number Z of small discrete vorticies $\Delta\Gamma_j$. The unit velocities induced by $\Delta\Gamma_j$ are given by

$$\left.\begin{aligned} cU_{mn} &= \frac{1}{2t}\frac{\sin\frac{2\pi}{t}(y_m - y_n)}{\cosh\frac{2\pi}{t}(x_m - x_n) - \cos\frac{2\pi}{t}(y_m - y_n)} \\ V_{mn} &= -\frac{1}{2t}\frac{\sinh\frac{2\pi}{t}(x_m - x_n)}{\cosh\frac{2\pi}{t}(x_m - x_n) - \cos\frac{2\pi}{t}(y_m - y_n)} \end{aligned}\right\} \ . \tag{8}$$

The numerical analysis is conducted over a series of small discrete time steps Δt for each of which a discrete vortex element $\Delta\Gamma_j$ is shed from each body surface element which, for a typical element j , will be of strength

$$\Delta\Gamma_j = \gamma(s_j)\mathrm{d}s_j \ . \tag{9}$$

The right-hand side of the basic governing equation, i.e., equation (7) thus includes the influence of the superimposed uniform stream W_∞ plus the vorticity already shed into the mainstream flow. In the author's previous publications [1] to [3], for cascades the assumption was made that each blade flow was indentical, a not unreasonable assumption for unstalled turbine or fan blade rows. However, for off-design angles of attack leading to stall it is well known that there can be significant blade-to-blade

variations particularly in fan and compressor cascades and the aim here is to extend the analysis to deal with such situations. We will deal with this in the next section.

3. **Revised cascade modelling**

Adaption of the previous vortex cloud model to allow simulation of at least some blade-to-blade variations is in fact relatively simple and is as illustrated in Figure 3.

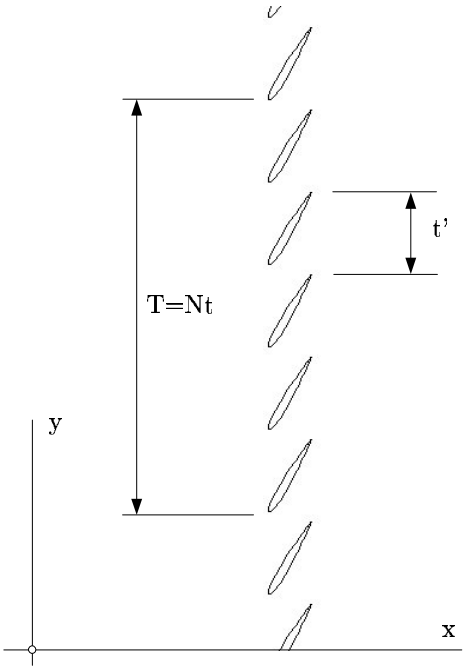

Figure 3. Revised model for the cascade with N independent blade profiles and group pitch T.

The approximation here is that there are N independent blades, (in this example 5) and that the flow pattern will thus repeat at the revised cascade pitch $T = Nt$. The group of $N = 5$ blades selected here may then be regarded as a single body shape when making up the $K(s_m, s_n)$ matrix of equations (7). The blade pitch t in equations (4) and (8) is then replaced by the group pitch T. In effect we are now analysing the flow through a group of N separate bodies, but cascaded as a group at pitch T in the y direction. Choice of the group size N is then a matter of computational limitations including available memory, time of execution and numerical accuracy available for inversion of the large $K(s_m, s_n)$ matrix. The outcome is best illustrated at this point by a typical solution as shown below in Figure 4.

Figure 4. Simulation of deep propagating stall through a fan cascade at high angle of attack.

The fan cascade shown here consists of five C4 profiled blades with zero camber θ, a stagger angle of $\lambda = 60^o$ and a pitch/chord ratio $t/l = 1.0$. We note that the predicted pattern is repeated after every five normal blade pitches t as indicated by the repeated blade numbering from 1 to 5.

The inflow angle β_1 of 85^o for this example corresponds to 25^o angle of attack and is naturally excessive, ensuring a state of deep stall. The outcome of this is well known but none the less remarkable. After a period of time as the motion proceeds, we observe the development of a large stall cell actually upstream of the blade row which propagates in the vertical direction. The reason for this behaviour can be deduced from the vortex dynamics simulation demonstrating the power of this CFD technique for prediction and diagnosis. Thus we may observe that the major blockage of the blade passage at position 2 due to the stall cell is causing increased flow through the passages adjacent to blade 5 due to the consequent decrease in angle of attack of the blades behind the moving stall cell. Shortly blade No.1 will also begin to unstall as the cell proceeds upward. Thus blades 4,5 and 1 are delivering a pressure rise locally across the blade row whereas the adjacent blades 2 and 3 are totally stalled. The outcome of this is that the stagnant fluid in the blade passages adjacent to blade 2 is blown upstream to augment the developing upstream stall cell causing a periodic fluctuation and thus likely strong aerodynamic excitation of the blades.

In this example there were only five independent blade profiles resulting in one large stall cell. In practice there could be several cells developing and propagating and one simulation with ten independent blades of a compressor cascade undertaken by the author revealed two cell regimes, i.e. one every 5 blade pitches. This situation is illustrated in the next example to be investigated in Section 4, namely the case of a radial diffuser.

4. **Extension to radial diffusers**

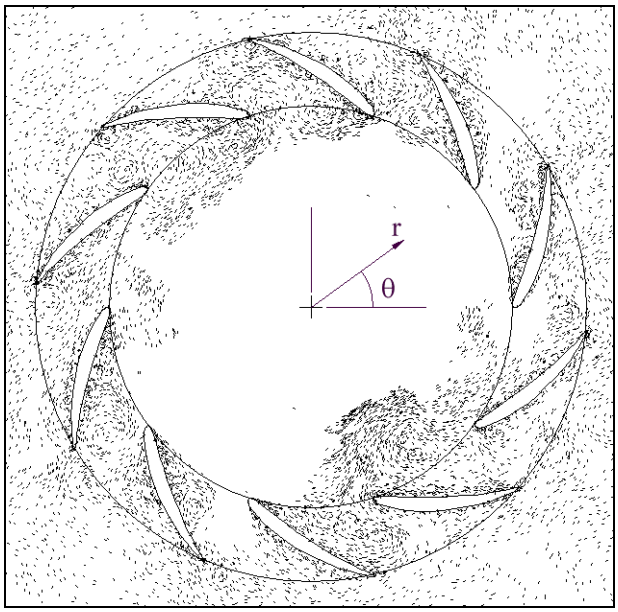

Figure 5. Simulation of deep stall in a radial outflow diffuser with ten blades.

Because the distributed vorticity of the mainstream flow has been replaced in the numerical model by a cloud of discrete vorticies, it is valid to apply conformal transformations to the linear cascade and its flowfield provided the vortex element strengths $\Delta\Gamma$ remain unchanged. Thus the previous analysis may be applied directly to radial stators by means of the following transformation [3][4] between a radial diffuser in the Z plane and a rectilinear cascade parallel to the η axis in the ζ plane,

$$\zeta = \ln Z \ , \tag{10}$$

where $Z = re^{i\theta}$ and $\zeta = \xi + i\eta$. The coordinate and velocity transformations are then given by

$$\xi = \ln r, \qquad \eta = \theta \ , \tag{11a}$$

$$q_\zeta = q_Z r \ , \tag{11b}$$

where r, θ are polar coordinates of the actual radial blade row.

Figure 5 shows the outcome of applying this transformation to analysis of a ten bladed radial outflow diffuser. The blade geometry in the cascade ζ plane is identical to that used in Section 3, namely a C4 base profile with $\theta = 0^o$, $\lambda = 60^o$, $t/l = 1.0$ and with a pre-whirl inlet angle $\beta_1 = 85^o$ (anti-clockwise outflowing swirl). For this computation the number of blades was set at $N = 10$ to achieve full simulation of flow through the radial diffuser.

The main observation to note here is the development of two major rotating stall cells on the upstream (inner) side of the diffuser. These are not identical but very similar in size and extent and are found to precess around the inner region in the well known manner of rotating stall in axial compressors and fans. At circumferential locations between the two stall cells the blades are less stalled (and sometimes temporarily unstalled) due to their increased local distribution of the mass flow and hence reduced local angles of attack. In these regions pressure recovery through the diffuser is achieved resulting in higher pressure surrounding the exit regions. This higher pressure forces the stagnant fluid in the stall cell regions to be pushed back inwards with a consequent build up of the stall cells and a perpetuation of the large scale disturbances. In the case of a centrifugal fan it can be expected that these stall cells would cause serious fluctuating interference with the rotor and be a serious source of unwanted vibrations.

It is of considerable interest to extend these studies from radial stators to radial rotors since in the latter we would expect the additional influence of work input including those due to relative eddy and Coriolis forces. The question raised then is whether these additional effects would enhance stall cell development or inhibit it. Fortunately all the relevant equations to handle this have already been derived [3] and applied to potential flow through radial and mixed-flow turbomachines. To summarise, the governing equation (7) develops into the extended form

$$\left.\begin{aligned} \sum_{n=1}^{M} K(s_m, s_n)\gamma(s_n) = &-U_\infty \cos\beta_m \\ &- \left[V_\infty + \Omega\left\{r^2 - \tfrac{1}{2}\left(r_1^2 + r_2^2\right)\right\}\right] \sin\beta_m \\ &- \sum_{j=1}^{Z} \Delta\Gamma_j (U_{mj}\cos\beta_m + V_{mj}\sin\beta_m) \end{aligned}\right\}, \tag{12}$$

where the new middle line includes the influence of blade row rotation with angular speed Ω. From the appearance of this term $\Omega\left\{r^2 - \frac{1}{2}\left(r_1^2 + r_2^2\right)\right\}$ one can immediately detect that it represents the additional influence upon the flow due to Coriolis accelerations of fluid particles as they pass through the rotor and one might anticipate some considerable influence upon the consequent flow. This is indeed the case as we shall see from the following example.

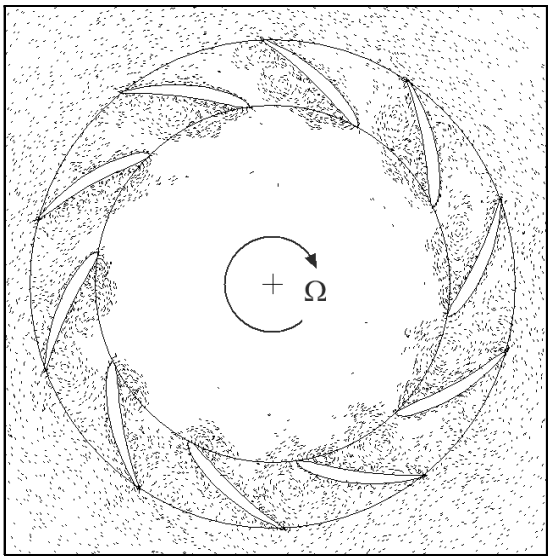

Figure 6. Flow through a backward sloping radial fan with relative inlet angle $\beta_1 = 85^o$.

In this example the previous blade row as shown in Figure 5 was rotated clockwise as a radial fan rotor with zero prewhirl but with sufficient angular velocity Ω to deliver the same relative inflow angle of β_1=85 $^\circ$ and thus 25 $^\circ$ angle of attack. A summary of the data is as follows:

Table 1. Design data for radial fan

Inlet radius r_1	1.0 m
Outlet radius r_2	1.3691 m
Meridional velocity at r_1	1.0 m/s
Angular velocity	109.15 revs/min
Prewhirl angle α_1	0 $^\circ$
Relative inlet angle β_1 at r_1	85 $^\circ$
Camber θ	0 $^\circ$
Stagger λ	60 $^\circ$
Pitch/chord ratio t/l	1.0
Time step Δt	0.005 sec

As can be seen from the predicted flow pattern after 300 time steps, Figure 6, although there is clear evidence of stall with some circumferential variation from blade to blade, there has been no establishment of the upstream eddy regimes characteristic of the stationary blade row, Figure 5. It is quite clear that the presence of Coriolis accelerations and relative eddy effects have had a major stabilising effect in the case of this radial fan rotor as compared with its stator equivalent Figure 5.

5. **Axial compressor type blade rows**

In the foregoing fan *uncambered* blade row studies it was difficult to detect classical cascade stall propagation or regular rotating stall in the radial diffuser at smaller angles of attack. Although some stall propagation was present below 15^o angle of attack it was largely intermittent. It was decided therefore to consider also a typical axial compressor blade row with the following specification.

Table 2. Axial compressor cascade design data

Chord length	1.0 m
Velocity normal to cascade	1.0 m/s
Camber θ	44.49 °
Stagger λ	41.11 °
Pitch/chord ratio t/l	1.162
Design inlet angle β_1	54.59 °
Predicted design outlet angle β_2	30.69 °

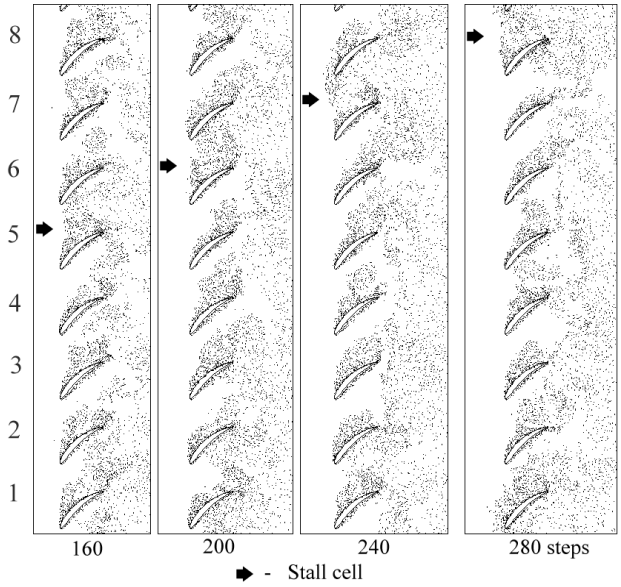

Figure 7. Stall propagation in a compressor cascade (Table 2 data with β_1=74.59 ° & δt=0.015)

Adopting here the cascade geometry studied in refs. [5]&[6], we note the introduction of typical camber θ=44.49^o and stagger λ=41.11^o. The design inlet angle given above is that for shock-free inflow for which the inlet stagnation point is precisely on the leading edge. Vortex cloud analysis was undertaken with a time step δt=0.015s for angles of attack of 0, 5, 10, 15 and 20^o angle of attack above this for a cascade-with eight independent blades. Only for the last of these studies, with an inlet angle

β_1=74.59 $^\circ$, was regular stall propagation actually found to develop in this cascade and a sample of the results is shown in Figure 7.

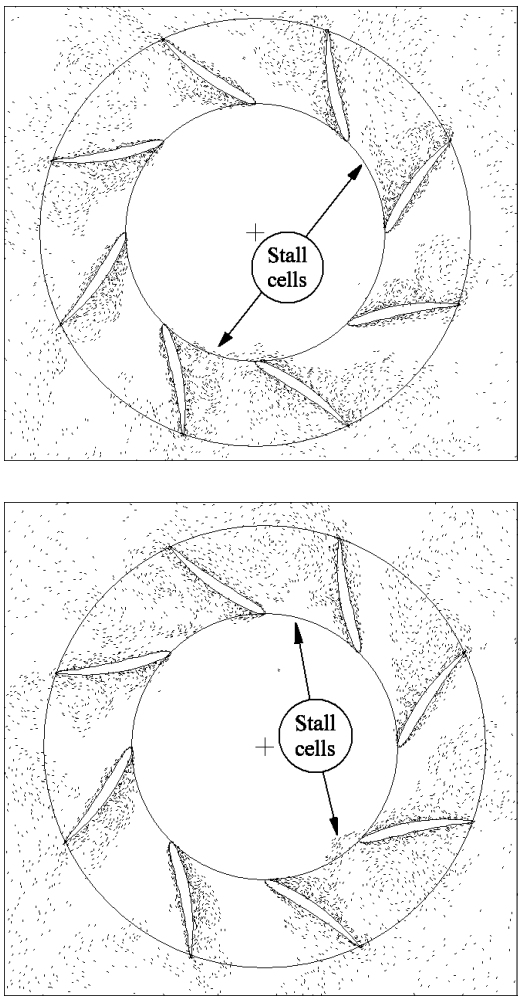

Figure 8. Development of rotating stall cells in an eight bladed 'axial compressor type' radial diffuser

As may be observed, after 160 time steps a stall cell has built up in blade passage No. 5. After successive intervals of 40 time steps this stall cell has propagated upwards to blade passages 6, 7 and 8. It should be noted that this pattern behaviour was found to occur only with 20^o angle of attack. At lower inlet angles there was evidence of developing stall progagation but with less firm regularity.

To conclude, let us consider adaption of the above cascade geometry for design of an equivalent radial diffuser. Application of the conformal transformation equations (10)

and (11) results in the circular radial outflow cascade shown in Figure 8. Adopting an inlet prewhirl angle of β_1=74.59^o, with time steps of magnitude $\delta t = 0.015$ and a meridional velocity at the inlet radius r_1 of value 1.0, the predicted flow pattern after 300 and 335 time steps is shown in Figures 8(a) and 8(b), respectively.

We observe from Figure 8 the presence of a single passage stall cell at the bottom region which has moved anticlockwise into the next blade passage after 35 time steps. We also note, however, the presence of a second but less concentrated cell located at the top of the diffuser also rotating anticlockwise at the same speed. Reference back to Figure 7 in fact reveals the presence of a similar second stall cell region around passage 1 to begin with, moving upwards to passage 4 finally. The main difference fluid dynamically between the two axial and radial cascades lies in the influence of viscous diffusion. For infinite Reynold's number viscous effects would have little influence. For the cascade Reynold's number of 1×10^5 selected here on the other hand, viscous diffusion will differ considerably due to the additional mainstream radial diffusion in the case of the radial diffuser. Despite this, stall cell propagation is remarkably similar for both cases considered comparing Figures 7 and 8.

To conclude finally, the flow through the previous cambered radial blade row was investigated when used as a radial fan rotor with two speeds of rotation, Figure 9.

Figure 9(b) shows the typical long term flow pattern for Ω=34.644revs/s, at which angular velocity zero prewhirl α_1 provides the same relative inlet angle as the stator just considered in Figure 8, β_1=74.59^o. Figure 9(a), on the other hand, shows the predicted flow pattern for half this speed of rotation, Ω=17.322 revs/s, but with sufficient prewhirl α_1=61.15^o to give the same relative inlet angle β_1=74.59^o. Three important observations may be made:

(a) Although some rotating stall still occurs, there is decreasing evidence of major stall cells as the rotor angular velocity increases.
(b) Major separation seems to be limited largely to the leading edge region with evidence of what seems to be an approach towards reattachment at mid-chord on the trailing surface t.
(c) From mid-chord towards the trailing edge region there is evidence of migration of diffused vorticity from the trailing surface t to the leading surface l, indicated by M in Figure 9(b).

Undoubtedly the explanation for the above is the influence of Coriolis accelerations upon the relative flow through these radial rotors. Specific work input due to associated Coriolis forces is dependent only upon the radial shift of the fluid from inlet r_1 to outlet r_2 and the rotor angular velocity Ω as shown by the Euler Pump Equation, namely

$$\left.\begin{array}{rcl} \frac{1}{\rho}\,(p_{02}-p_{01}) \;=\; U_2c_{\theta 2} - \;U_1c_{\theta 1} & = & \Omega(r_2c_{\theta 2}-r_1c_{\theta 1}) \\ = \quad \underbrace{\Omega(r_2w_{\theta 2}-r_1w_{\theta 1})}_{\substack{\text{Aerodynamic}\\ \text{specific work input}}} \quad + \quad \underbrace{\Omega^2(r_2^2-r_1^2)}_{\substack{\text{Coriolis specific}\\ \text{work input}}} & & \end{array}\right\}, \tag{13}$$

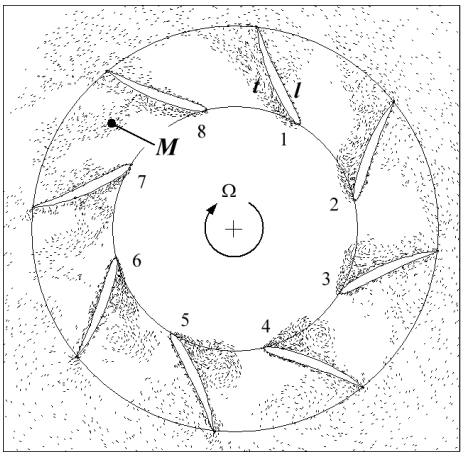

$\Omega = 17.322$revs/s, Prewhirl angle α_1=61.15^o 280 iterations with δt=0.015.

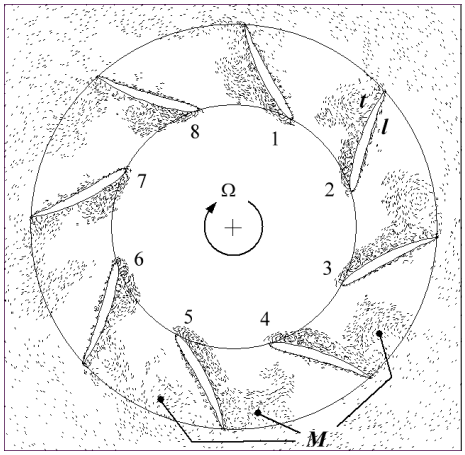

$\Omega = 34.644$revs/s, Prewhirl angle α_1=0.0^o, 360 iterations with δt=0.01.
l - leading surface. t - trailing surface.
M - Circumferential vorticity migration.

Figure 9. Flow through the radial diffusing blade row operating as a radial fan rotor

where w_θ is the swirl velocity measured relative to the rotor, and is related to the absolute swirl velocity c_θ through

$$c_\theta = w_\theta + r\Omega \, . \tag{14}$$

It is clear that although there is leading edge flow separation due to the sharp angle of attack, the specific work input imposed by Coriolis effects has a stabilising effect as the fluid proceeds further through the blade passages. However, partly due to

the anticlockwise 'relative eddy rotation' or 'slip flow' in the passage exit region, free vorticity tends to migrate from where it has been created on the unstable trailing surface t towards the leading surface l.

6. **Conclusions**

The following summary of conclusions may be drawn from these fluid dynamic developments and studies:

1. The basic linear cascade vortex dynamics code developed here has successfully predicted the presence of rotating stall in fan and compressor cascades in agreement with earlier work.
2. At high incidence angles in deep stall, substantial stall cells intrude back upstream of the blade row.
3. A conformal transformation technique has succeeded in extending these flow simulations to deal with radial blade rows used as either stators or rotors.
4. At large relative inlet angles a couple of large rotating deep-stall cells were found to develop on the inlet side of a radial outflow diffuser stator comprising a backward swept zero camber fan cascade at high stagger.
5. For the cambered compressor type radial diffuser stator no deep-stall cells of this kind developed for the same leading edge angle of attack of 20^o, although rotating stall was present.
6. For the same blade row employed as a radial fan rotor, work input due to Coriolis forces leads to general stabilization of the initial leading edge stall regime. The same 'relative eddy' effects result in vorticity migration at the outlet radii from the trailing (highly loaded) blade surface towards the (generally low velocity) leading edge surface.

REFERENCES

1. Lewis, R.I.: Development of vortex dynamics for simulation of turbomachine cascades and blade rows. *Journal of Computational and Applied Mechanics*, **2**(1), (2001), 73-85.
2. Lewis, R.I.: Extension of vortex methods to the flow simulation of mixed-flow turbomachines. *Proc. of the Second International Conference on Vortex Methods*, Istanbul, Turkey, Sept 2001.
3. Lewis, R.I.: *Vortex Element Methods for Fluid Dynamic Analysis of Engineering Systems*. Cambridge University Press, 1991.
4. Lewis, R.I.: Vortex element methods, the most natural approach to flow simulation - a review of methodology with applications. *Proceedings of the First International Conference on Vortex Methods*, Kobe, Japan, (1999), 1-15.
5. Chunjun Ji: *Vortex Cloud Method and its Applications to Turbomachine Cascades*. Ph.D. Thesis, Newcastle University, 1997.
6. Lewis, R.I. and Chunjun Ji: Extension of vortex cloud modelling to cylinder arrays and cascades in relative motion. *Proceedings of the Fourth European Computational Fluid Dynamics Conference*, Athens, pp. 642-647, J. Wiley & Sons, 1998.